Egypt. J. Chem. **Vol. 67**, No. 10 pp. 413 - 427 (2024)

Egyptian Journal of Chemistry

http://ejchem.journals.ekb.eg/

Assessment of Azolla Microphylla Plant Extract as an Environmentally Benign Corrosion Inhibitor for Low-Carbon Steel in Acidic Media

Medhat M. Kamel [1, *], Mohamed A. Ghanem[2*], Abdel Aziz S. Fouda[3*], Salah M. Rashwan[1], Osama Abdelkader[1], Nasser Y. Mostafa[1], Khaled M. H. Mohammed[4]

[1] Department of Chemistry, Faculty of Science, Suez Canal University, Ismailia, 41522, Egypt.*
[2] Department of Chemistry, College of Science, King Saud University, Riyadh 11451, Saudi Arabia.*
*[3 *]Department of Chemistry, Faculty of Science, Mansoura University, Mansoura, Egypt.*
[4] School of Chemistry, University of Southampton, Southampton SO17 1BJ, United Kingdom.

Abstract

In this study, Azolla Microphylla Extract (AME) appears as a potent corrosion inhibitor, effectively reducing the corrosion rate of low-carbon steel (CS) in a 1.0 M HCl solution. Comprehensive investigation methods, including weight loss (WL), potentiodynamic polarization (PP), electrochemical impedance spectroscopy (EIS), and electrochemical frequency modulation (EFM), were employed. The inhibition efficiency (IE) was evaluated across a range of extract concentrations (50-300 ppm) and temperatures (298-313 K). There is a good agreement between the results of the electrochemical and WL methods. A remarkable IE of 98.1% was achieved at 313 K with 300 ppm of AME, displaying its effectiveness. At 298 K, the IE was 81.3%. Adsorption of AME on CS followed Langmuir isotherm and at temperatures of 308 K or lower, the ΔG^{o}_{ads} magnitudes were below -20 kJ mol^{-1}, indicative of physical adsorption. However, at 313 K, ΔG^{o}_{ads} exceeded –20 kJ mol^{-1}, signalling a change to chemical adsorption. AME belongs to the anodic inhibitors. The activation energy for the blank solution is 98.13 kJ mol^{-1}, which decreased to 62.98 kJ mol^{-1} in the presence of 300 ppm of AME. Nyquist plots showed that AME inhibited CS dissolution in HCl without altering the dissolution reaction mechanism. Attenuated total reflection infrared (ATR-IR) and scanning electron microscopy (SEM) inspections confirmed the adsorption of AME on CS. AME satisfies the general structural requirement of the corrosion inhibitor as it has O atoms in functional groups (O-H, C=C, and C=O) and an aromatic ring. The findings align well with other environmentally friendly inhibitors previously reported for CS corrosion.

Keywords: Azolla Microphylla, Plant extract, Corrosion, Inhibitor, Low-carbon steel. HCl media.

1. Introduction

Corrosion, defined as the degradation of materials due to interactions with the surrounding environment, poses a significant challenge in various industrial applications. The corrosive environment, whether chemical or electrochemical, coupled with mechanical stresses, can lead to the reversion of metallic materials to their lower internal energy [1]. The widespread use of carbon steel, formed by the combination of steel and carbon, in industrial processes such as petrochemical operations, acidic pickling, oil recovery, and crude oil refinement, underscores the importance of addressing corrosion-related issues [2].

Hydrochloric acid (HCl) is extremely employed in industrial descaling and scrubbing procedures, where the corrosive nature of carbon steel in acidic environments becomes a prominent concern. Inhibitors play a crucial role in inhibiting the corrosion of steel under such conditions [3]. While varieties of organic compounds have anti-corrosive properties; their synthesis often incurs prohibitive costs and environmental risks. Consequently, there is a growing emphasis on environmentally benign compounds, with researchers focusing on utilizing readily available, renewable, and biodegradable sources like plant extracts, which are considered green inhibitors [4-6]. Plant extracts, abundant in polyphenols, flavonoids, tannins, alkaloids, and polysaccharides, have shown potential for suppressing metal corrosion [7, 8]. Extracts from various plant parts, including bark, fruits, leaves, seeds, and roots, contain organic components with N or O atoms that form a protective film on the metal

*Corresponding author e-mail: medhat_darwish@science.suez.edu.eg, (Medhat M. Kamel)
Receive Date: 16 March 2024, Revise Date: 16 April 2024, Accept Date: 24 April 2024
DOI: 10.21608/ejchem.2024.277352.9465

surface, inhibiting corrosion [9-11]. Several studies have explored the application of natural substances as effective inhibitors for steel corrosion in diverse environments, yielding positive results [12-16].

1.

Natural substances derived from sources like Stachys byzantine leaves [12], Piper betel [13], Ziziphora [14], Ficus racemosa [15], Banana peel [16], Terminalia catappa [17], Holoptelea integrifolia [18], Luffa cylindrica [19], Aganonerion polymorphum [20], Mish gush [12], Olives [21], Pigeon pea seed [22], Aquilaria [23], Syzygium samarangense [24], natural Lettuce oil [25], natural Parsley oil [26], Spinacia oleracea [27], expired Lactulose drugs [28], and Cinnamon [29] have demonstrated effectiveness in reducing steel corrosion rates. These natural products create strong interactions with the steel surface through electrostatic forces and/or chemical bonding involving positive ions of steel and heteroatoms or polar groups, such as COO^-, CN^-, NH_2^-, OH^-, SH^-, and phenyl groups. Hence, plant-based solutions offer potential developing, eco-friendly, and potent corrosion inhibitor systems [30].

Azolla microphylla, an aquatic fern belonging to the Salvinaceae family, is recognized as a "golden green mine" and is found in freshwater bodies globally [31]. Traditionally, it has been used as a biofertilizer in rice fields. Azolla creates a symbiotic relationship with a cyanobacterium called Anabaena azollae [32]. With the help of this cyanobacterium, atmospheric nitrogen may be fixed and transformed into ammonia, which plants can use [32]. This relationship causes Azolla to become highly nitrogenous. Research shows that its dry-weight nitrogen content can range from 2 to 5% [32]. Azolla functions as a natural fertilizer for rice plants by breaking down and releasing fixed nitrogen into the soil when it is added to a rice field. Azolla is a sustainable and environmentally beneficial choice because it lessens the demand for artificial nitrogen fertilizers [33]. This macrophyte has diverse applications, including animal feed for fish, pigs, and poultry birds [34, 35]. Rich in proteins, vitamins, akaloids, and bioactive flavonoids [36], Azolla microphylla is the focal point of this study.

This research aims to assess the inhibition performance of Azolla microphylla extract (AME) on carbon steel (CS) corrosion in a 1.0 M HCl solution. Utilizing various methodologies such as WL, PP, EIS, and EFM, we investigate the adsorption behavior of AME on the CS surface. The study explores the influence of temperature on inhibition effectiveness and employs ATR-IR and SEM techniques to examine the surfaces of CS samples with and without AME extract. To our knowledge, this study represents the first comprehensive examination of AME extract as a novel green inhibitor.

2. Materials and methods

2.1 CS samples

Prior to conducting any measurements, the CS coupons were polished using emery papers of varying grades, ranging from 600 to 1200. The composition of coupons included 0.28% C, 0.087% P, 0.22% Si, 0.6% Mn, 0.081% Cr, 0.20% Cu, 0.07% S, 0.11% Ni, and 0.31% Sn, with the remaining being Fe. For weight-loss measurements, samples with dimensions of 2.0 × 2.0 × 0.2 cm^3 were carefully cleaned with double-distilled water, followed by degreasing with acetone, and subsequently air-drying at room temperature before precise weighing [36].

The specimens chosen for electrochemical measurements were prepared by drying them at room temperature, exposing only a defined area of 1 cm^2, with the remaining surface treated with epoxy resin. Subsequently, it air-dried at ambient temperature before precise weighing [37].

2.2 Preparation of a blank solution

Analytical-grade HCl (32%) was diluted with double-distilled water to prepare the corrosive medium of 1.0 M HCl. All tests were performed on stagnant solutions.

2.3 Preparation of Azolla microphylla plant extract (AME)

An electrical mill running at room temperature was used to grind the dried Azolla microphylla plant into a fine powder. In a soxhlet extraction apparatus, about 200 g of the powder were soaked in 800 ml of methanol. After that, the extract was concentrated in a rotary evaporator and kept in a sterile, airtight container. As proposed by Onipe *et al*. [38], the extract was dissolved in ethanol (1 g/L) and then put in a refrigerator for the activation step. ATR-IR was employed to figure out the main functional groups, which were found in the extract, prior to and after the corrosion test.

2.4 Measurement techniques

2.4.1Weight-loss measurements

The uniformly sized, polished CS specimens were tied with threads and submerged in a 100 ml test solution with varying inhibitor (AME) concentrations for 180 minutes. After that, the CS specimens were cleaned and dried, and the weight loss was computed [39].

$$CR = \frac{\Delta W}{At} \qquad (1)$$

Where *CR* stands for corrosion rate (mg cm^{-2} min^{-1}), ΔW is the average decrease in weight in mg, *A* is the area in cm^2, and *t* is 180 minutes. The inhibition efficiency (IE_w) was calculated using equation (2) [40].

$$IE_w = \frac{CR - CR_i}{CR} \times 100 \quad (2)$$

Where *CR* and CR_i represent the corrosion rates, respectively, in the absence and presence of AME.

2.4.2 Electrochemical studies

The PP studies were conducted with the help of a Gamry Instrument (PCI 4-G750). The experiments were conducted in a traditional cell assembly using a typical calomel reference electrode (SCE), a Pt gauze counter electrode, and a CS specimen of 1 cm^2 as a working electrode (WE). The latter was immersed in the corrosive medium for 30 minutes before each run to reach a constant open-circuit potential. At a scan rate of 1 mV s^{-1}, the polarization was swept from -1000 mV (vs. SCE) to 0 mV (vs. SCE).

The inhibition efficiency (IE_p) and the surface coverage (θ) were estimated from polarization measurements based on the following relations [41].

$$IE_p = (1 - \frac{i_{(inh)}}{i_{(free)}}) \times 100 \quad (3)$$

$$\theta = (1 - \frac{i_{(inh)}}{i_{(free)}}) \quad (4)$$

Where, $i_{(free)}$ and $i_{(inh)}$ are the corrosion current densities in the non-existence and existence of AME.

AC impedance spectra were recorded using the same apparatus that was used for the polarization investigation. Also, the cell arrangement was the same. An AC signal with a peak-to-peak amplitude of 10 mV and a wide range of frequency (100 KHz to 10 mHz) was used for EIS. The capacitance of the double layer (C_{dl}) was computed by equation (5) [42].

$$C_{dl} = Y_o(\omega_{max})^{n-1} \quad (5)$$

Where Y_o is the coefficient of proportionality, $\omega_{max} = 2\pi f_{max}$, f_{max} is the frequency at which the imaginary component (Z_{imag}) attains a maximum, and *n* is the shift in phase. The inhibiting efficiency (IE_{EIS}) of corrosion is computed from the magnitudes of R_{ct} based on the following relationship [42].

$$IE_{EIS} = \frac{R_{ct} - R_{ct}^o}{R_{ct}} \times 100 \quad (6)$$

Where R_{ct} is the charge transfer resistance in the presence of AME and R_{ct}^o is the charge transfer resistance in blank solution.

Two separate frequencies, 2 and 5 Hz, were used for EFM measurements. Every second, the waveform refreshes itself at its smallest frequency of 0.1 Hz. The spectrum shows both harmonically attributable current responses and inter-modification current peaks. The Tafel slopes, corrosion current, and causality factors were all computed utilizing the higher peaks [42]. The inhibition efficiency *(IE_{EFM})* and θ can be computed from equations (7) and (4), respectively.

$$IE_{EFM} = (1 - \frac{i_{(inh)}}{i_{(free)}}) \times 100 \quad (7)$$

2.5 ATR-IR analysis

In the presence and absence of 300 ppm of AME at room temperature, the CS samples were immersed in 100 ml of 1.0 M HCl. After 24 hours, the samples were carefully removed and air-dried. Subsequently, the CS sample's surface coating underwent meticulous scratching, and the obtained samples were subjected to ATR-IR spectrum testing. A Thermo Fisher Scientific Nicolet IS10 model with a wavenumber range of 400- 4000 cm^{-1} was employed for ATR-IR measurements to ascertain the composition of the corrosion product formed on the CS surface.

2.6 Surface analysis

The examination of the CS sample's surface, both in the presence and absence of the highest concentration of AME (300 ppm) following immersion for 24 h at room temperature, was conducted using a JEOL JSM-5500 scanning electron microscope.

3. Results and discussion

3.1 ATR-IR analysis of AME

ATR-IR spectroscopy, chosen for its advantages including a high signal-to-noise ratio, selectivity, sensitivity, simplicity, precision, quick processing times, and minimal sample requirements, proved to be a cost-effective tool for researchers. Prior to the corrosion test, the IR spectra of AME alone were recorded. Subsequently, by carefully scratching the coupons, the IR spectra of the films adsorbed on the CS surface were obtained, as illustrated in Fig. 1. The analysis of AME revealed the presence of various functional groups at specific wavelengths, including 3422 cm^{-1} (O-H stretch) [43, 44], 2923 cm^{-1} (C-H stretch), 1400 cm^{-1} (C-C stretch (in-ring) aromatics), 1087 cm^{-1} (C-N stretch aliphatic amines), and 611 cm^{-1} (-C (triple bond) C-H: C-H bend alkynes) [45]. The strong band at 1639 cm^{-1} is assigned to C=C and C=O stretching vibrations. Owing to the conjugation effect of flavonoids in Azolla microphylla, the C=O peak shifts from about 1700 cm^{-1} to a lower wave number (1639 cm^{-1}). The C=C and C=O stretching vibration bands are in superposition [46]. The adsorption bands at 1452 and 1122 cm^{-1} could be assigned to the framework vibration of an aromatic ring. Previous studies by Nnanna and Owate [46] highlighted that the presence of carbonyl and double bonds containing carbon groups in plant extracts signifies features capable of corrosion inhibition. The spectra of AME after interaction with the CS surface

displayed bands at 3333 cm^{-1} (O-H stretch), 2923 cm^{-1} (C-H stretch), and 1636 cm^{-1} (C=O bending), with shifts suggesting potential interactions between these functional groups of the Azolla extract (adsorbate) and the CS metal ions [47]. According to these findings, AME satisfies the general structural requirement of the corrosion inhibitor since it has O atoms in functional groups (O-H, C=C, and C=O) and an aromatic ring [46].

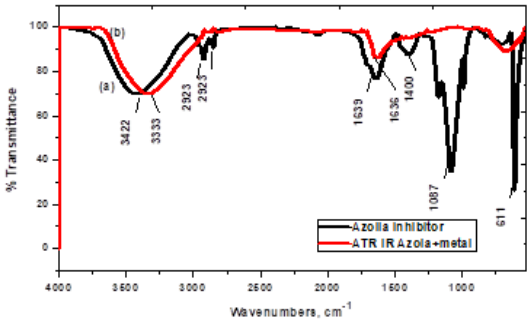

Fig. 1. ATR-IR spectra of AME before (a) and after (b) corrosion in 1.0 M HCl.

3.2 SEM of test CS coupons

Fig. 2 illustrates the characteristics of the polished CS surface under different conditions: the polished CS surface (Fig. 2a), the CS surface immersed in 1.0 M HCl for 24 hours without an inhibitor (Fig. 2b), and the CS surface immersed in 1.0 M HCl for 24 hours in the presence of 300 ppm of AME at room temperature (Fig. 2c). Before exposure to acidic environment, the SEM image of the polished CS coupon reveals a smooth and compact surface (Fig. 2a). However, after 24 h of immersion in 1.0 M HCl, the CS coupon shows the formation of permeable layers with microcracks, showing the susceptibility of the CS surface to corrosion (Fig. 2b). Notably, the aggressive ions (Cl^- and H_3O^+) readily penetrate the CS, leading to corrosion of the coupon. In contrast, when AME is introduced into the acidic environment (Fig. 2c), the CS surface shows significant improvement in smoothness, reduced porosity, and fewer microcracks, all indicative of a slower corrosion rate. The observed enhancement in surface morphology can be attributed to the formation of a protective shielding film by AME on the metal surface. This highlights the strong adsorption propensity of AME on the CS surface, proving it an efficient inhibiting agent for CS in acidic media.

3.3 WL tests and the effect of temperature

WL assessment, a traditional, non-electrochemical technique, can be utilized to predict the distinct properties and corrosion rates of an inhibitor. Compared to the electrochemical approach, it offers data that is more correct and trustworthy. This is mostly because the experimental conditions used are set up and executed in a more convincing manner, but the intervals or test periods take a long time [2]. Therefore, it would be clear that the acquired values differed from the electrochemical values based on the characteristics and discrepancies in the experimental nature.

The *CR* and IE_w were calculated by using equations (1) and (2), respectively. The IE_w of Azolla microphylla extracts under different conditions is illustrated in Table 1. The inhibition level was enhanced, and the rate of corrosion decreased when the AME dosage rose because the active AME molecules (concentration-dependent) spontaneously adhered to the CS surface, blocking mass transfer processes and preventing further metal dissolution [48]. At 300 ppm and 313 K, the inhibition reached 98.1%. This implies that the process of adsorption involving the adsorbate (AME) and the CS surface has been sufficiently proven and leads to the formation of a dense metal-inhibitor interaction. Consequently, it prevents chloride ions (Cl^-) from accumulating on the steel's face layer [22]. The impact of temperature on the IE_w was studied at different doses of the AME, as seen in Table 1. An increase in temperature increases the percentage of IE_w, implying that chemisorption is followed by AME adsorption on the CS surface [49].

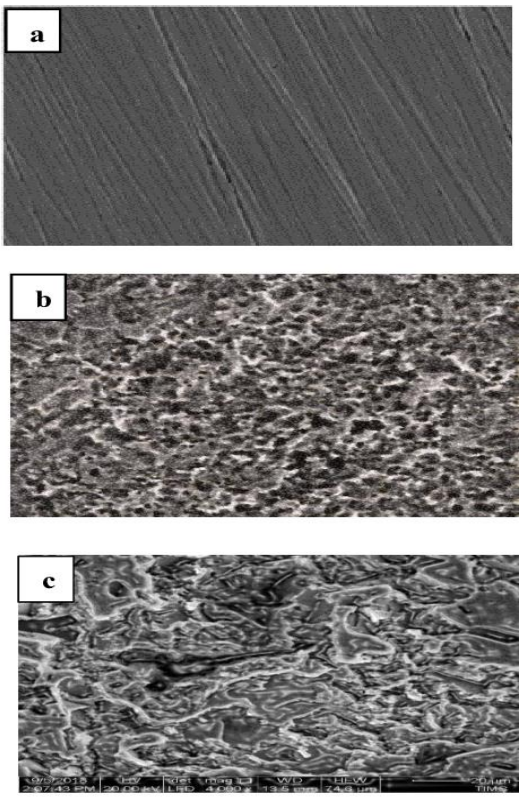

Fig. 2. SEM images of (a) polished CS, (b) CS after exposure to 1.0 M HCl (blank), and (c) CS after exposure to 1.0M HCl + 300 ppm of AME at room temperature. The exposure time is 24 hours.

Table 1. WL measurements for CS in 1.0 M HCl in the absence and presence of various concentrations of AME at 298-313 K.

Concn. (ppm)	Temp. (K)	CR (mg cm^{-2} min^{-1})	θ	IE$_w$ (%)
Blank	298	0.008	-	-
	303	0.015		
	308	0.054		
	313	0.084		
50	298	0.006	0.250	25.0
	303	0.005	0.667	66.7
	308	0.004	0.926	92.6
	313	0.002	0.976	97.6
100	298	0.005	0.375	37.5
	303	0.004	0.733	73.3
	308	0.0035	0.935	93.5
	313	0.002	0.976	97.6
150	298	0.004	0.500	50.0
	303	0.0035	0.767	76.7
	308	0.0028	0.948	94.8
	313	0.002	0.976	97.6
200	298	0.003	0.625	62.5
	303	0.0025	0.833	83.3
	308	0.0014	0.974	97.4
	313	0.0012	0.978	97.8
250	298	0.002	0.750	75.0
	303	0.0015	0.900	90.0
	308	0.0013	0.976	97.6
	313	0.0012	0.978	97.8
300	298	0.0015	0.813	81.3
	303	0.0011	0.927	92.7
	308	0.0011	0.979	97.9
	313	0.0010	0.981	98.1

3.4 Thermodynamic activation parameters

Thermodynamic parameters are noteworthy tools for understanding inhibitor/extract adsorption behaviour. For the dissolution of CS in a 1.0 M HCl solution, the activation energy (E_a^*), enthalpy change (ΔH_a^*), and entropy change (ΔS_a^*) of activation were computed [36]. The parameters were estimated both in the existence and non-existence of the AME by Arrhenius and transition-state equations.

$$k = A\ exp\left(\frac{-Ea^*}{RT}\right) \qquad (8)$$

$$ln\left(\frac{K}{T}\right) = \left(ln\left(\frac{k_B}{h}\right) + \left(\frac{\Delta S^*}{R}\right)\right) - \frac{\Delta H^*}{RT} \qquad (9)$$

Where k is the corrosion rate, A is the Arrhenius factor, R is the universal gas constant, k_B is the Boltzmann constant, T is the Kelvin temperature, and h is the plank's constant. The Arrhenius plot $(log\ k\ vs.\ \frac{1}{T})$ and the transition state plot $(ln\frac{K}{T}\ vs.\ \frac{1}{T})$ of the AME are shown in Figs. 3 and 4, respectively. The Arrhenius plot shows a straight line with a slope of $\frac{-Ea^*}{2.303R}$, from which the E_a^* for the corrosion process is computed (Table 2). The value of the E_a^* for the blank solution is 98.13 kJ mol^{-1}. The activation energy dramatically decreases as the AME concentration rises because the extract inhibits corrosion by chemically adhering to the CS surface. A larger value of E_a^* indicates a physisorption mechanism, whereas an unaltered or lower E_a^* in the inhibiting system relative to the blank is supportive of a chemisorption mechanism and forms stronger bonds between the inhibitor and CS [50]. The decrease in E_a^* values with increasing AME concentration is evidence for the inhibitor's effectiveness.

Plots of transition states show a straight line with a slope of $\left(\frac{-\Delta H_a^*}{2.303R}\right)$ and an intercept $(log\ (\frac{k_B}{h}) + (\frac{\Delta S_a^*}{R}))$, which is used to calculate ΔS_a^* and ΔH_a^* (Table 2). The positive ΔH_a^* values indicate the endothermic nature of the activated complex formation during the corrosion process. Analyzing the trend of ΔS_a^* with increasing AME concentration refers to the fact that initially positive ΔS_a^* signifies increased disorder as inhibitor molecules initially interact and occupy sites. However, negative ΔS_a^* at higher concentrations suggests an ordering effect, where inhibitor molecules arrange themselves in a more structured film, leading to a more protected surface and hindering corrosion further. Furthermore, the transition state's activated complex shows an interaction rather than a dissolution phase, suggesting that the ordering happens throughout the transition from the reactants to the activated complex [11]. The trend of decreasing E_a^* and the transition from positive to negative ΔS_a^* with increasing AME concentration illustrate how the AME progressively inhibits corrosion by forming a more organized protective film on the CS surface.

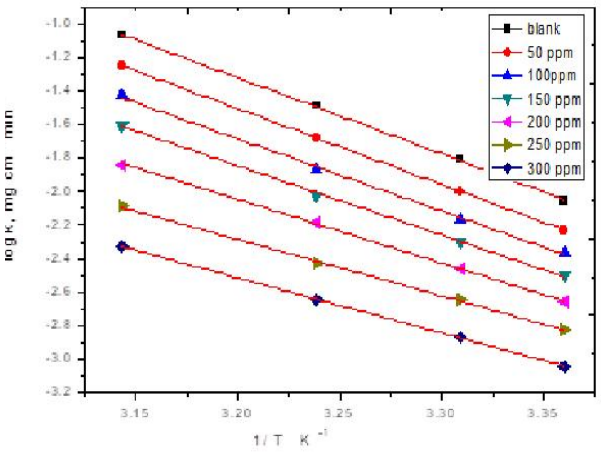

Fig. 3. Arrhenius plots for CS corrosion in 1.0 M HCl in the absence and presence of different concentrations of AME.

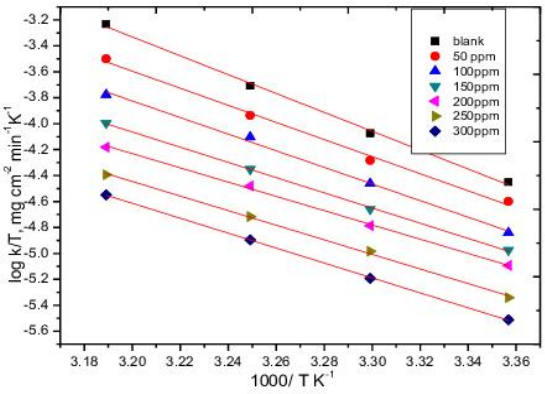

Fig. 4. Transition state plots for CS in 1.0 M HCl in the absence and presence of different concentrations of AME.

Table 2. Activation parameters for CS in the absence and presence of different concentrations of AME in 1.0M HCl.

Concentration (ppm)	E_a^* (kJ mol^{-1})	ΔH_a^* (kJ mol^{-1})	ΔS_a^* (J mol^{-1} k^{-1})
Blank	98.13	52.65	81.40
50	86.65	37.63	50. 90
100	82.55	35.85	34.30
150	79.28	34.42	20.70
200	72.81	31.62	-3.70
250	64.68	28.08	-34.3
300	62.98	27.35	-260.5

3.5 Adsorption model and thermodynamics study

Corrosion inhibition has been considered to begin with the adsorption phenomenon, in which molecules of inhibitor tend to adsorb on the corroding surface layer. In this study, the most suitable adsorption mode was examined using the conventional weight loss method to find the extent of surface coverage filled by AME molecules *(θ)*. To provide more insight into the inhibiting impact of AME on the CS surface, the Langmuir model with high fitting (R^2 ranging between 0.991 and 0.995) was put forth (Fig. 5), and its applicability was evaluated using equation (10) [22].

$$\frac{C_{inh}}{\theta} = \frac{1}{K_{ads}} + C_{inh} \qquad (10)$$

Where K_{ads} is the equilibrium constant for the adsorption process, C_{inh} is the concentration of AME, and θ is the surface layer filled by AME molecules. Plotting (C_{inh}/θ) as a function of C_{inh} clearly shows a mathematical model of a straight-line equation with values for the slope and intercept, respectively, as Fig. 5 illustrates. In general, the data fits well with the Langmuir model. The slopes of the lines slightly deviate from the value of one due to lateral interactions between adsorbed molecules [51,52]. Table 3 provides the estimated K_{ads} derived from the reciprocal of the isothermal line intercept. Increasing the temperature from 298 to 313 K tends to increase the K_{ads} value from 3.9 to 117.6 due to the change of adsorption type from physical to chemical. The high values of K_{ads} indicate that the adsorbed film is strong and stable [53]. Also, AME adsorption becomes more favourable at higher temperatures. It is worth observing a decreasing trend in the intercept value of the Langmuir plot with increasing temperature (Table 3). This implies a smaller amount of AME is needed to achieve the same level of surface coverage *(θ)* at higher temperatures. This can be explained by the stronger driving force for adsorption at higher temperatures, leading to a more efficient occupation of available sites on the CS surface.

Equation (11) refers to the relationship between the adsorption equilibrium constant (K_{ads}) and the standard Gibbs energy change (ΔG^o_{ads}) for the adsorption process [54].

$$\Delta G^o_{ads} = -RT \ln(55.5\ K_{ads}) \qquad (11)$$

Where T is the absolute temperature, R is the gas constant, and 55.5 is the water concentration in molarity units. Using the Van't Hoff equation, the adsorption heat, ΔH^o_{ads}, can be calculated [54].

$$lnK_{ads} = \left(\frac{-\Delta H^o_{ads}}{RT}\right) + constant \qquad (12)$$

The calculation of ΔH^o_{ads} is based on the slope of the correlation between $(ln\ K_{ads}$ and $1/T)$, which equals $-\Delta H^o_{ads}/R$. Equation (13) is used for quantifying the entropy change (ΔS^o_{ads}) of the AME adsorption.

$$\Delta G^o_{ads} = \Delta H^o_{ads} - T\Delta S^o_{ads} \qquad (13)$$

Table 3 shows the obtained values of ΔS^o_{ads}. The ΔS^o_{ads} increase from -32.55 to -0.638 J/K as the temperature increases from 298 to 313 K. The negative magnitudes of ΔG^o_{ads} signify the stable state of the adsorbed film on the CS surface as well as the spontaneous action of the separated molecules during the adsorption process at different temperatures. The more negative the value, the greater the thermodynamic driving force for adsorption. The AME molecules are strongly adsorbed onto the CS surface, as shown by all the negative values. At higher temperatures, AME molecules in the solution have greater kinetic energy. This allows them to overcome the activation energy barrier for adsorption onto the CS surface more readily. ΔG^o_{ads} magnitudes of about -20 kJ mol^{-1} or less are associated with electrostatic interaction between charged molecules and the charged metal (physisorption); values of about -40 kJ mol^{-1} or higher represent charge sharing or the distribution of organic molecules to the metal surface to develop a coordinate form of bond (chemisorption) [54]. Values positioned in between the two adsorption

modes are suggestive of a mixed physiochemical mechanism. In this study, ΔG^{o}_{ads} values in the range of −13.3 to −22.8 kJ mol^{-1} show that mixed physicochemical adsorption verifies the AME adsorption process on CS in a 1.0 M HCl solution. The extract's adsorption is accompanied by a heat evolution, as indicated by the negative value of ΔH^{o}_{ads} [55]. Unlike the typical trend for adsorption processes (increased order leading to negative ΔS^{o}_{ads}), the values of ΔS^{o}_{ads} become less negative (closer to zero) with increasing temperature. This could be due to the ordering effect of AME molecules arranging on the CS surface, which might be counterbalanced by some increased mobility and freedom of movement within the adsorbed layer at higher temperatures. In addition, the increased temperature might influence the behaviour of water molecules at the interface between the CS surface and the AME layer, leading to a more complex interplay between order and disorder.

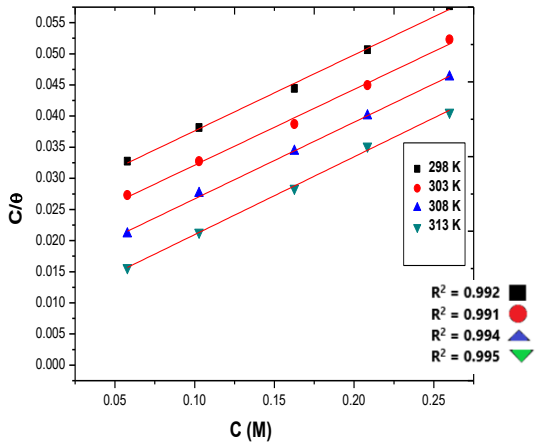

Fig. 5. Langmuir adsorption curves for CS in 1.0 M HCl with different concentrations of AME at different temperatures (298-313 K).

Table 3. Adsorption parameters of AME on CS in 1.0 M HCl at different temperatures.

Temp. (K)	Slope	Intercept	K_{ads} M^{-1}	-ΔG° kJ mol^{-1}	-ΔH° kJ mol^{-1}	ΔS° J mol^{-1} K^{-1}
298	1.09	0.256	3.9	13.3		-32.55
303	1.18	0.208	4.8	14.1	23.00	-29.37
308	1.17	0.144	6.9	15.2		-25.32
313	1.12	0.0085	117.6	22.8		-0.638

3.6 PP study

For electrochemical measurements, a volume of 500 ml of the extracted solution (1 g/L of ethanol) was accurately diluted to 1liter by doubly distilled water to form a stock solution with a concentration of 500 parts per million (ppm). The stock solution was then diluted to the desired concentration (50–300 ppm) with the proper amount of doubly distilled water. Fig. 6 shows the PP of the CS electrode after 30 minutes of submerging in the examined solutions with 0-300 ppm of AME. When CS was exposed to the blank solution, significant corrosion developed. The presence of aggressive ions, such as Cl^- and H_3O^+, in the corrosive media speeds up the dissolution of CS. Fortunately, the addition of AME to the corrosive solution resulted in significant decreases in current densities, which decreased the corrosion rate of the CS. As the concentration of AME increases, the anodic and cathodic branches of the observed polarization curves gradually move toward the lower current density, indicating a decrease in the overall corrosion rate [56]. The shape of anodic and cathodic branches was changed, showing that AME addition governed both anodic and cathodic reactions. The evolution of hydrogen is shown by the cathodic polarization curves; however, the dissolution of CS is expressed by the anodic polarization curves [55]. Adding 300 ppm of AME to the solution resulted in more cathodic polarization and protective film development on the anodic branches. By managing both anodic and cathodic reactions, these phenomena may lead to a noticeable drop in corrosion current densities, indicating that the addition of AME could be capable of reducing CS corrosion in the acidic pickling solution. Table 4 displays corrosion parameters including E_{corr} (corrosion potential), I_{corr} (corrosion current density), and β_a and β_c (anodic and cathodic Tafel slopes), respectively, calculated from Tafel extrapolation [57]. The anodic and cathodic branches were almost linear and symmetrical within ± 200 mV around E_{corr} , where both Tafel slopes were extrapolated. The lines intersected at E_{corr} where all corrosion variables were measured. The IE_p and surface coverage (θ) were calculated according to equations (3) and (4), respectively.

The type of corrosion inhibitor is identified using the obtained E_{corr}. The inhibitor can act as either a cathodic or anodic type if the E_{corr} value is greater than 85 mV relative to the blank solution, and as a mixed type if the E_{corr} value is less than 85 mV. For the present study, The difference between E_{corr} in the presence of AME (300 ppm) and in the blank solution is 224 mV (Table 4). As the anodic Tafel slope (β_a) is more affected by the addition of AME than cathodic Tafel slope, AME is therefore an anodic inhibitor [56]. An anodic inhibitor preferentially adsorbs on the metal surface, hindering the oxidation (dissolution) of the metal. This can lead to a shift in the corrosion potential towards more positive values (anodic shift) as the driving force for metal dissolution is reduced.

The findings show that in the 1.0 M HCl solution, I_{corr} significantly decreases as the AME concentration increases. When AME concentration increased, inhibition performance improved as a result. Table 4

displays data revealing a significant decrease in current density upon the addition of AME. The efficiency of inhibition improves to 79.7% as the concentration of extract increases to 300 ppm at 298 K. Slower kinetics on the active sites caused by increased AME addition may facilitate the development of a protective film on the CS surface [10]. More specifically, when the concentration of AME is adequate, an entirely protective coating may form on the surface of the CS, improving its resistance to corrosion.

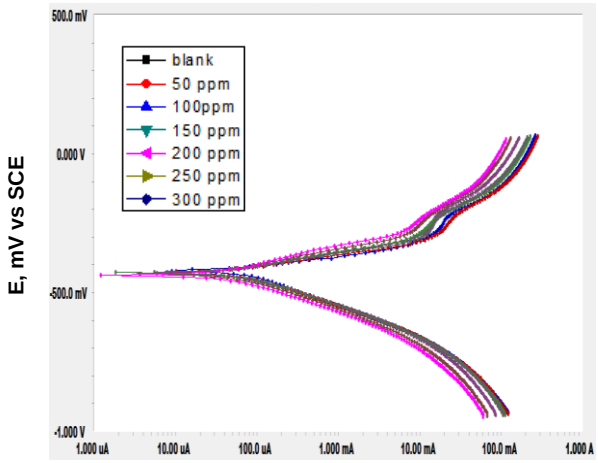

Fig. 6. PP curves c and presence) M HCl in the absence ions of AME at 298 K.

Table 4. PP values of CS in 1.0 M HCl in the absence and presence of different concentrations of AME at 298 K.

Concn. (ppm)	E_{corr} (mV)	$I_{corr}\times 10^{-3}$ (mA/cm^2)	β_a (mV/decade)	$-\beta_c$ (mV/decade)	θ	IE_p (%)
Blank	-527	404	89.9	121.7	-	-
50	-442	300	140.1	133.2	0.257	25.7
100	-324	260	108.6	139.6	0.356	35.6
150	-385	200	144.5	123.6	0.504	50.4
200	-315	160	103.2	118.3	0.604	60.4
250	-307	103	139.4	120.1	0.745	74.5
300	-303	82	143.6	130.2	0.797	79.7

3.7 EIS study

In the examined solutions having 0-300 ppm of AME, Fig. 7(a) shows the EIS response in the Nyquist plots (Z_{real} as real impedance versus $-Z_{imag}$ as imaginary impedance) of a corroding film-covered CS. A small value of impedance together with a depressed semicircle reveals significant corrosion of CS immersed in the blank solution, characterized by an extensive hydrogen bubble on the CS. The semicircle in the studied solution expanded when AME was added, and the impedance values increased with the AME concentration. The Nyquist plots showed that a higher concentration of AME increased the charge transfer resistance (R_{ct}), which in turn improved the corrosion resistance of CS in the 1.0 M HCl solution. The semicircles' diameter and shape changed dramatically when AME was added to the blank solution, showing that the protective film completely formed on the CS surface. The calculated electrochemical variables, including R_{ct} and C_{dl}, are provided in Table 5. Equation (6) was used to calculate the IE_{EIS}.

Notably, C_{dl} values decrease with increasing AME concentration, indicating that the adsorption mechanism is best described by the Helmholtz model. Fig. 7(b) shows the EIS response in the Bode plots, including phase angle and impedance versus frequency in the studied solutions. The spectra that were recorded at high, medium, and low frequencies signify imperfections on the CS surface, processes via the protective film (or the rust layer), and the interface between the CS and protective film, respectively [15]. The protective film and the CS/protective film interface were significantly affected by the addition of AME, as shown by the spectra in the Nyquist and Bode plots, which showed notable alterations at medium and low frequencies. The Bode plot shows that as AME concentrations increased, so did the impedance and the phase angle shift, which resulted in a more capacitive surface coating. The outcomes shown by the Nyquist and Bode plots match as well. The equivalent circuit in Fig. 7(c) is provided for simulating and matching the EIS findings of CS in a 1.0 M HCl solution, both without and with the addition of AME, based on the EIS spectra. It consists of R_s (solution resistance), C_{dl} (capacitance), and R_p (polarization/charge transfer resistance).

Table 5. EIS parameters for corrosion of CS in 1.0 M HCl in the absence and presence of different concentrations of AME at 298 K.

Concn. (ppm)	R_{ct} (Ω cm^2)	C_{dl} (F cm^{-2})	θ	IE_{EIS} (%)
Blank	40.7	6.70×10^{-4}	-	-
50	55.1	1.83×10^{-4}	0.261	26.1
100	62.2	1.94×10^{-5}	0.345	34.5
150	80.6	1.86×10^{-5}	0.495	49.5
200	106.4	1.44×10^{-5}	0.617	61.7
250	163.8	1.23×10^{-5}	0.752	75.2
300	208	0.89×10^{-5}	0.804	80.4

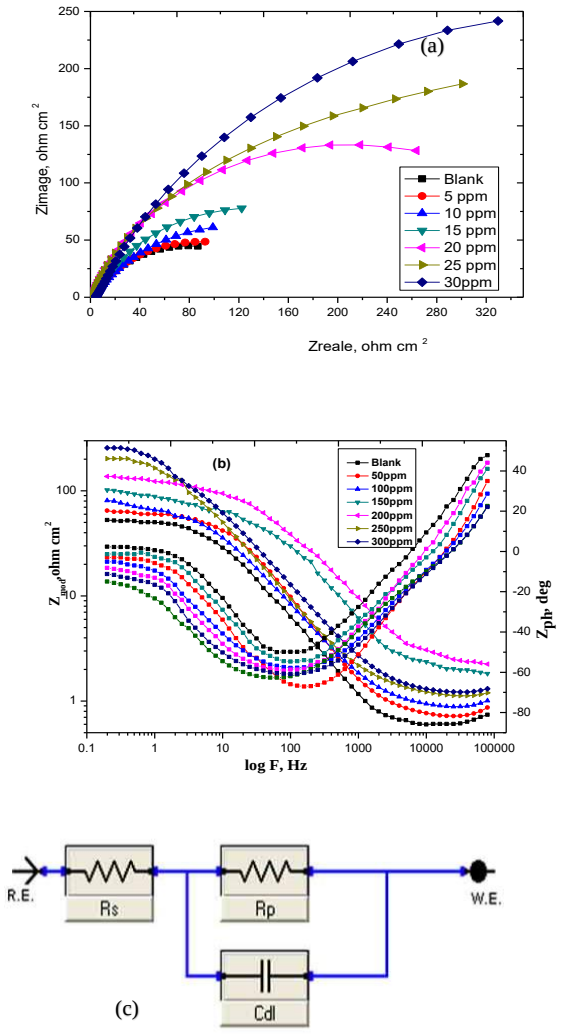

Fig. 7. The Nyquist (a) and Bode (b) plots of the CS in 1.0 M HCl in the absence and presence of different concentrations of AME at 298 K. (c) the electrical equivalent circuit used to model the results of EIS.

3.8 EFM study

The EFM spectra of CS corrosion in 1.0 M HCl, both in the existence and non-existence of 300 ppm of AME, are displayed in Fig. 8. The current response includes the given input frequencies and components of frequency. The frequency components are produced by dividing, multiplying, and adding the two given input frequencies. The two major peaks of the response to the stimulating frequencies are found at 0.2 and 0.5 Hz. The Tafel slopes, the corrosion current, and the causality factors (CF-2 and CF-3) are all computed using the major peaks [58]. Table 6 displays the Tafel constants, inhibition efficiency, and causality factors for various AME concentrations at 298 K. The I_{corr} reduces and the IE_{EFM} improves with increasing AME dose in the corrosive media. This is caused by the protective film that is formed at the CS surface, which reduces the dissolution of metal. When the AME interacts with the adsorbed Cl^- anions, adsorption occurs. The values of the causality factors have a direct correlation with theoretical values 2 and 3. This implies that the data obtained is quite good [59].

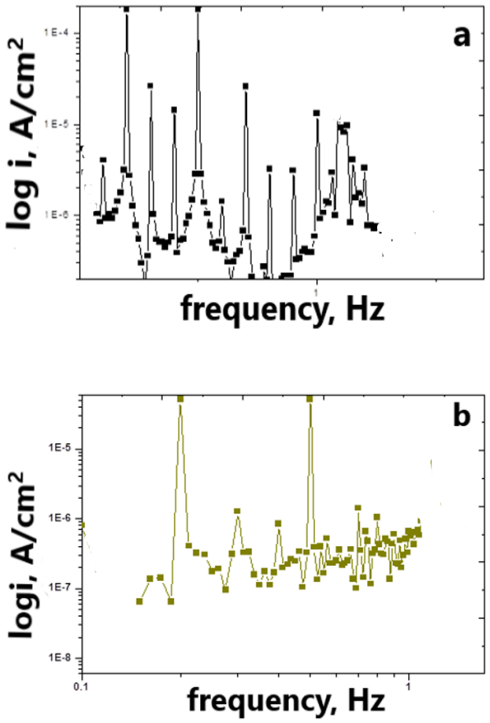

Fig. 8. EFM spectra for the corrosion of CS in 1.0 M HCl in the absence (a) and presence of 300 ppm of AME (b) at 298 K.

Table 6. EFM parameters of CS in 1.0 M HCl in the absence and presence of different doses of AME.

Concn. (ppm)	$I_{corr}\times10^{-3}$ (mA/cm^2)	$-\beta_c$ (mV/decade)	β_a (mV/decade)	CF-2	CF-3	θ	E_{EFM} (%)
Blank	422	98	126	2.2	2.90	-	-
50	306	111.6	140.1	1.91	3.13	0.262	26.2
100	263	138.4	148.5	1.87	2.77	0.375	37.5
150	204	144.7	111.6	1.82	2.83	0.521	52.1
200	164	103.2	101.3	2.08	2.97	0.633	63.3
250	101	101.6	120.1	2.07	3.10	0.711	71.1
300	80	120.6	107.3	1.98	2.88	0.812	81.2

3.9 Mechanism of corrosion inhibition

According to the experimental results, AME molecules inhibited the corrosion of CS in a 1.0 M HCl electrolyte. The adsorption process and the constituents' structures reported in the AME can be used to understand the probable mechanism of inhibition. The structures of the major components of AME, which include 2,3,4,5,2',6'-Hexamethoxy-4',5'-methylenedioxychalcone, and 9-Octadecenoic acid, are shown in Fig. 9. Due to the many chemical bonds, heteroatoms, and carbonyl groups in the two configurations, they are adsorbed on the metal surface [60, 61].

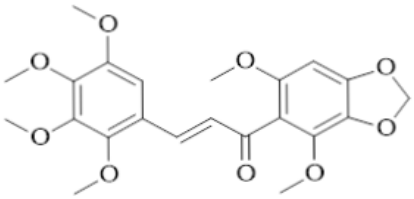

2,3,4,5,2',6'-Hexamethoxy-4',5'-methylenedioxychalcone

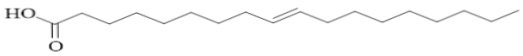

9-Octadecenoic acid

Fig. 9. The major phytoconstituents of AME**.**

In the presence of HCl solutions, the anodic reactions of iron can be summarized as follows [56]:

$$Fe + H_2O + Cl^- \rightarrow [FeClOH]^-_{ads} + H^+ + e^- \quad (14)$$

$$[FeClOH]^-_{ads} \leftrightarrow [FeClOH]_{ads} + e^- \ (rate\ determining\ step) \quad (15)$$

$$[FeClOH]_{ads} \leftrightarrow Fe^{2+} + H^+ + H_2O \quad (16)$$

In oxygenated acidic chloride solutions, the cathodic reaction is [62]:

$$4H^+ + O_2 + 4e \rightarrow 2H_2O \quad (17)$$

The addition of the organic inhibitor to the HCl solution leads to the formation of a thin film on the metal surface and therefore decreases the rate of corrosion. This results from a substitution reaction between molecules of inhibitor and molecules of water at the metal/solution interface. Equation (18) describes the substitution reaction between organic inhibitor and water molecules [56].

$$xH_2O_{(ads)} + Org_{(sol)} \Rightarrow Org_{(ads)} + xH_2O_{(sol)} \quad (18)$$

Where $H_2O_{(sol)}$ and $H_2O_{(ads)}$) are molecules of water in solution and absorbed water molecules on the metal surface, respectively. $Org_{(sol)}$ and $Org_{(ads)}$ are molecules of inhibitor dissolved in solution and inhibitor molecules adsorbed on the metal surface, respectively. The size ratio, or *x*, is the number of molecules of water that one organic inhibitor molecule displaces. Notably, the organic inhibitor's shape affects the size ratio. An organic inhibitor with planar geometry offers higher coverage of the surface and accordingly functions more effectively as a corrosion inhibitor [56].

Since the rate of adsorption is often high, the acid solution (HCl) is kept away from the reactive CS surface [5]. Chemical structure, molecular size, the type of metal and its charged surface, and the distribution of charge throughout the inhibitor molecule all affect an inhibitor's ability to adsorb. In general, two adsorption types (chemisorption and physisorption) were taken into consideration. By displacing water molecules from the CS surface and sharing electrons between the heteroatoms and CS, the chemisorption mechanism allows the neutral molecules of AME to be adsorbed on the surface of CS. Additionally, the inhibitor molecules may adsorb on the surface of the CS through donor-acceptor interactions between the unoccupied d-orbitals of the CS surface and the π-electrons of the aromatic/heterocyclic ring (retrodonation).

It is commonly known that in acidic solutions, the CS surface is positively charged [63]. Consequently, the electrostatic repulsion makes it hard for the protonated plant molecules to get close to the positively charged CS surface (H_3O^+/metal interface). Since chloride ions are less hydrated than other ions, they can generate extra negative charges near the interface. As a result, they make it possible for the protonated plant extract to adsorb via electrostatic interactions (physisorption) on the negatively charged CS surface. Fig.10 illustrates the mechanism of inhibition.

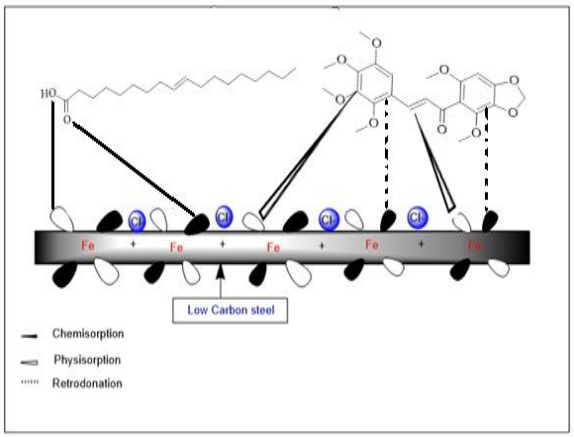

Fig. 10. Schematic figure of carbon steel corrosion inhibition in 1.0 M HCl solution in the presence of AME.

3.10 A comparison of the inhibition efficiency of AME alongside different natural extracts in the literature for CS corrosion

The results of a comparison between the inhibition efficiency found in this investigation and that of other recognized green inhibitors are displayed in Table 7. The outcome of this investigation was compared favourably with several green inhibitors used to treat CS.

Table 7. Comparison of the inhibition efficiency of AME with other natural inhibitors on CS.

Natural plant extract	Inhibition efficiency	Reference
Eriobotrya japonica thunb	90% in 1M HCl at 298 K	[3]
Strychnos nuxvomica	88.1% in 8% HCl at 298 K	[6]
Paprika	95% in 1M HCl at 313 K	[11]
Burghul	95% in 1M HCl at 313 K	[64]
Ficus Racemosa	88.9% in 0.1 M HCl at 298	[15]
Olive leaf	K	[21]
Dioscorea septemloba	53% in 0.1M HCl at 298 K	[65]
Pterocarpus	72% in 1M HCl at 298 K	[66]
santalinoides	90% in 1M HCl at 333 K	[67]
Pomegranate leaf	69.4% in 1M HCl at 298 K	[68]
Red algae halopitys	81.9% in 1M HCl at 298 K	[69]
Aloe vera gel	42.3% in 1M HCl at 298 K	[70]
Corchorus olitorius	95.93% in 1 M HCl at 298 K	[71]
Grewia bicolor jus	93.03% in 1 M HCl at 298 K	This study
Azolla microphylla	98.1% in 1M HCl at 313 K	

Conclusion

This study comprehensively investigated the potential of Azolla Microphylla Extract (AME) as a natural inhibitor for low carbon steel (CS) corrosion in 1.0 M HCl, employing different techniques, including weight loss (WL), electrochemical methods (PP, EIS, and EFM), and surface analyses (ATR-IR, SEM). An increase in both temperature and extract concentration enhanced the inhibition efficiency of the extract. The consistency seen between electrochemical and WL approaches further underscores the reliability of the results. At 300 ppm, the extract showed exceptional inhibitory activity, achieving a remarkable 98.1% efficiency at 313K after 3 h in corrosive media. ATR-IR spectra analysis revealed the presence of functional groups, including OH, C=O, and C=C, showing the involvement of these groups in the corrosion inhibition process. SEM investigations provided visual evidence of a protective film formed on the CS surface through inhibitor adsorption, contributing to improved surface morphology. The adsorption of the AME belongs to Langmuir type. The plant extract (AME) contained important components, such as 2,3,4,5,2',6'-Hexamethoxy-4',5'-methylenedioxychalcone, and 9-Octadecenoic acid, which helped AME exhibit excellent corrosion-inhibiting properties. According to PP measurements, AME acts as an anodic inhibitor. The adsorption mechanism of AME on CS appeared to involve a combination of physisorption and chemisorption. These findings collectively highlight the promising potential of AME as an effective and environmentally friendly corrosion inhibitor for CS in acidic media.

Conflicts of interest

There are no conflicts to declare.

Formatting of funding sources

Researchers Supporting Program, Project Number (RSP-2024R518), King Saud University, Riyadh, Saudi Arabia.

Acknowledgments

The authors would like to express their sincere gratitude to the Researchers Supporting Program, Project number (RSP-2024R518), King Saud University, Riyadh, Saudi Arabia.

References

[1] de Souza Morais WR, da Silva JS, Queiroz NM, de Paiva e Silva Zanta CL, Ribeiro AS, Tonholo J. Green corrosion inhibitors based on plant extracts for metals and alloys in corrosive environment: A Technological and Scientific Prospection. J Appl Sci 2023. https://doi:10.3390/app13137482.

[2] Amin MA, Mohsen Q, Mostafa NY, Al-Refaie A, Bairamov AK, Al-Maaesab S, Murillo EM, Al-Qahtani SA. Case study: Impact of amine containing organic compound on the corrosion and electrochemical behaviors of constructive alloys in linear alpha olefin environment. Int J Electrochem Sci (2014);9(12): 7552-73.

[3] Yang W, Wang Q, Xu K, Yin Y, Bao H, Li X, Niu L, Chen S. Enhanced corrosion resistance of carbon steel in hydrochloric acid solution by eriobotrya japonica thunb. leaf extract: electrochemical study. Materials (2017);10(8): 956. https://doi:10.3390/ma10080956.

[4] Bedir AG, Abd El-raouf M, Abdel-Mawgoud S, Negm NA, El Basiony NM. Corrosion inhibition of carbon steel in hydrochloric acid solution using ethoxylated nonionic surfactants based on Schiff base: electrochemical and computational investigations. ACS Omega (2021);6(6): 4300-12. https://doi:10.1021/acsomega.0c05476.

[5] Singh A, Ebenso EE, Quraishi MA. Corrosion inhibition of carbon steel in HCl solution by some plant extracts. Int J Corros (2012);2012 1-20. https://doi:10.1155/2012/897430.

[6] Soltani N, Tavakkoli N, Ghasemi M, Corrosion inhibition of low carbon steel by Strychnos nuxvomica extract as green corrosion inhibitor in hydrochloric acid solution. Int J Electrochem Sci (2016);11(10): 8827-47. https://doi:10.20964/2016.10.22.

[7] Hassannejad H, Barati A, Nouri A. The use of nanoemulsion-based strategies to improve corrosion

inhibition efficiency of thyme-based inhibitor. J Mol Liq (2019);296: 112110. https://doi:10.1016/j.molliq.2019.112110.
[8] Oguzie EE, Onuchukwu AI, Okafor PC, Ebenso EE. Corrosion inhibition and adsorption behaviour of Ocimum basilicum extract on aluminium. Pigm Resin Technol (2006);35(2): 63-70. https://doi:10.1108/03699420610652340.
[9] Noor EA. Potential of aqueous extract of Hibiscus sabdariffa leaves for inhibiting the corrosion of aluminum in alkaline solutions, J Appl Electrochem (2009);39(9): 1465-75. https://doi:10.1007/s10800-009-9826-1.
[10] Amin MA, Mohsen Q, Mostafa NY, El-Bagoury N, Al-Refaie A, Bairamov AK, Al-Maaesab S, Murillo EM, Al-Qahtani SA. Case study: Corrosion behavior of constructive alloys in linear alpha olefin environment, Int J Electrochem Sci (2014);9(5): 2631-48.
[11] Kamel MM, Fouda AS, Rashwan SM, Abdelkader O. Paprika extract: a green inhibitor for mitigating carbon steel disintegration in 1 M HCl pickling solution. Green Chem Lett Rev (2021);14(4): 600-11. https://doi:10.1080/17518253.2021.1985173.
[12] Shahini MH, Ramezanzadeh M, Ramezanzadeh B, Bahlakeh G. The role of ethanolic extract of Stachys byzantina's leaves for effective decreasing the mild-steel (MS) degradation in the acidic solution; coupled theoretical/experimental assessments. J Mol Liq (2021);329 115571. https://doi:10.1016/j.molliq.2021.115571.
[13] Trung DC, Pham TT, Minh QBP, Panaitescu C, Tran NQ, Anh HT, Bach LX, Nguyen Dang N. The use of Piper Betel leaf extract for forming a barrier layer on steel surface in hydrochloric acid solution. Prog Org Coat (2021);158 106340. https://doi:10.1016/j.porgcoat.2021.106340
[14] Dehghani A, Bahlakeh G, Ramezanzadeh B, Ramezanzadeh M. Potential role of a novel green eco-friendly inhibitor in corrosion inhibition of mild steel in HCl solution: Detailed macro/micro-scale experimental and computational explorations. Constr Build Mater (2020);245 118464. https://doi:10.1016/j.conbuildmat.2020.118464.
[15] Anh HT, Vu NSH, Huyen LT, Tran NQ, Thu HT, Bach LX, Trinh QT, Prabhakar Vattikuti SV, Nam ND. Ficus racemosa leaf extract for inhibiting steel corrosion in a hydrochloric acid medium Alex Eng J (2020);59(6): 4449-62. https://doi:10.1016/j.aej.2020.07.051.
[16] Bala Manikandan C, Balamurugan S, Balamurugan P, Lionel Beneston S. Weight reduction of motorcycle frame by topology optimization, J Achiev Mater Manuf Eng (2018);2(92): 67-77. https://doi:10.5604/01.3001.0012.9664.
[17] Pramudita M, Sukirno, Nasikin M. Performance of Terminalia catappa leaves extract as bio-corrosion inhibitor for mild steel in H_2SO_4 solution. IOP Conference Series: Mater Sci Eng (2020);796(1): 012059. https://doi:10.1088/1757-899x/796/1/012059.
[18] Bhuvaneswari SS, Kumudha D, Prabha T, Sivakumar T. Azolla pinnata R. Br. : An aquatic macrophyte as a potential therapeutic candidate. Ann Phytomed (2022);11(1). https://doi:10.54085/ap.2022.11.1.13.
[19] Ogunleye OO, Arinkoola AO, Eletta OA, Agbede OO, Osho YA, Morakinyo AF, Hamed JO. Green corrosion inhibition and adsorption characteristics of Luffa cylindrica leaf extract on mild steel in hydrochloric acid environment. Heliyon (2020);6(1): e03205. https://doi:10.1016/j.heliyon.2020.e03205.
[20] Van Hien P, Hoai Vu NS, Bach LX, Tran NQ, Dao VA, Trinh QT, Nam ND. Capability of Aganonerion polymorphum leaf-water extract in protecting hydrochloric acid induced steel corrosion. New J Chem (2019);43(39): 15646-58. https://doi:10.1039/c9nj04079j.
[21] Elhady S, Inan H, Shaaban M, Fahim IS. Investigation of olive leaf extract as a potential environmentally-friendly corrosion inhibitor for carbon steel. Sci Rep (2023);13(1): 17151. https://doi:10.1038/s41598-023-43701-x.
[22] Onukwuli OD, Anadebe VC, Nnaji PC, Okafor NA, Abeng FE, Chidiebere MA, Chukwuike VI, Uwaleke CC, Guo L. Effect of pigeon pea seed (isoflavone) molecules on corrosion inhibition of mild steel in oilfield descaling solution: electro-kinetic, DFT modeling and optimization studies J Ira Chem Soc (2021);18(11): 2983-05. https://doi:10.1007/s13738-021-02250-8.
[23] Sin HLY, Al-Shishani A, Abdul Rahim A, Saad B, Pandian BR. Corrosion inhibition potential of Aquilaria leaf constituents – A HPLC view. Prog Org Coat (2019);135 536-44. https://doi:10.1016/j.porgcoat.2019.06.022.
[24] Zhou Y, Zhu C, Xu S, Xiang B, Marzouki R. Combining electrochemical, surface topography analysis, and theoretical calculation methods to insight into the anti-corrosion property of Syzygium samarangense leaf extract. J Ind Eng Chem (2021);102: 302-11. https://doi:10.1016/j.jiec.2021.07.016.
[25] Abdallah M, Soliman KA, Alfakeer M, Al-bonayan AM, Alotaibi MT, Hawsawi H, Hazazi OA, Abdel Hameed RS, Sobhi M. Mitigation effect of natural lettuce oil on the corrosion of mild steel in sulfuric acid solution: chemical, electrochemical, computational aspects. Green Chem Lett Rev (2023); 16(1):2249019.https://doi.org/10.1080/17518253.2023.2249019.
[26] Abdallah M, Soliman KA, Al Jahdaly BA, Al-Fahemi JH, Hawsawi H, Altass HM, Motaweabd MS,

Al-Juaid SS. Natural parsley oil as a green and safe inhibitor for corrosion of X80 carbon steel in 0.5 M H_2SO_4 solution: a chemical, electrochemical, DFT and MC simulation approach. RSC Adv (2022); 12: 2959–71.doi: 10.1039/d1ra08855f rsc.li/rsc-advances
[27] Abdel Hameed RS, Aleid GhMS, Mohammad D, Badr MM, Huwaimel B, Suliman MSh, Alshammary F, Abdallah M. Spinacia oleracea extract as green corrosion inhibitor for carbon steel in hydrochloric acid solution. J Electrochem Sci (2022); 17: 221017, doi: 10.20964/2022.10.31
[28] Abdel-Hameed R, Qureshi MT , Abdallah M, Aljuhani E, Alzharani AA , Alfarsi A, Bakry AM, Bader Huwaimel B, Othman Farghaly O. Recycling of expired lactulose drugs as eco-friendly corrosion inhibitor for steel alloys in acidic environment: gravimetrical and electrochemical studies. Int J Electrochem Sci (2022); 17: 221270. https://doi: 10.20964/2022.12.92
[29] Abdallah M, Al-Fahemi JH, Soliman KA, Al-Gorair AS, Al-Sharif MS, Al-Juaid SS, Al Waness SA, Sobhi M. Exploring cinnamon extract's potential as a green corrosion inhibitor for X65 carbon steel in sulfuric acid: a comprehensive investigation. J Disper Sci Technol (2024), https://doi.org/10.1080/01932691.2024.2333537
[30] Rani BEA, Basu BBJ. Green inhibitors for corrosion protection of metals and alloys: an overview, Int J Corros (2012);2012: 1-15. https://doi:10.1155/2012/380217.
[31] Wagner GM. Azolla: a review of its biology and utilization. Bot Rev (1997);63(1): 1-26. https://doi:10.1007/bf02857915.
[32] Watanabe I, Roger PA, Ladha JK, Van Hove C. Biofertilizer germplasm collections at IRRI, (1992), International Rice Research Institute, Manilla 1099, Phillippines.
[33] Carrapico F, Teixeira G, Diniz MA. Azolla as a biofertilizer in Africa, A challenge for the future. Revistade Ciencias Agrarias (2000); 23 (3-4): 120-38.
[34] Lumpkin TA, Plucknett DL. Azolla: botany, physiology, and use as a green manure, Econ Bot (1980);34(2): 111-53. https://doi:10.1007/bf02858627.
[35] Abraham G, Aeri V. A preliminary examination of the phytochemical profile of Azolla microphylla with respect to Seasons. Asian Pac J Trop Biomed (2012);2(3): S1392-95. https://doi:10.1016/s2221-1691(12)60423-7.
[36] Fouda A, Rashwan S, Abdelfatah M. Corrosion inhibition of stainless steel 304 in hydrochloric acid solution using clindamycin antibiotic as eco-friendly inhibitor. Zast mater (2019);60(1): 3-17. https://doi:10.5937/zasmat1901003f.
[37] Abdallah M, Asghar BH, Zaafarany I, Fouda AS. The inhibition of carbon steel corrosion in hydrochloric acid solution using some phenolic compounds. Int J Electrochem Sci (2012);7(1): 282-04. https://doi:10.1016/s1452-3981(23)13338-4.
[38] Onipe OO, Jideani AIO, Beswa D. Composition and functionality of wheat bran and its application in some cereal food products. Int J Food Sci Tech (2015);50(12): 2509-18. https://doi:10.1111/ijfs.12935.
[39] Usman AD, Victoria AF, Okoro LN. Weight loss corrosion study of some metals in acid medium. J Adv Chem (2016);11(2): 3434-40. https://doi:10.24297/jac.v11i2.2211.
[40] Verma C, Quraishi MA, Ebenso EE, Bahadur I. A green and sustainable approach for mild steel acidic corrosion inhibition using leaves extract: experimental and DFT studies. J Bio Tribo Corros (2018);4(3). https://doi:10.1007/s40735-018-0150-3.
[41] Rybalka KV, Beketaeva LA, Davydov AD. Estimation of corrosion rate of AISI 1016 steel by the analysis of polarization curves and using the method of measuring ohmic resistance. Russ J Electrochem (2021);57(1):16-21. https://doi:10.1134/s1023193521010092.
[42] Lemallem SE, Fiala A, Ladouani HB, Allal H. Corrosion inhibition performance of two ketene dithioacetal derivatives for stainless steel in hydrochloric acid solution, J Electrochem Sci Technol (2022);13(2): 237-53. https://doi:10.33961/jecst.2021.00822.
[43] Mostafa NY, Qhtani MM, Alotaibi SH, Zaki ZI, Alharthi S, Cieslik M, Gornicka K, Ryl J, Boukherroub R, Amin MA. Cathodic activation of synthesized highly defective monoclinic hydroxyl-functionalized ZrO_2 nanoparticles for efficient electrochemical production of hydrogen in alkaline media. Int J Energy Res (2020);44(13): 10695-09. https://doi:10.1002/er.5713.
[44] El-Moemen AA, Shata SA, Pashameah RA, AlSubhi SA, Alzahrani E, Farouk AEA, Zaki ZI, Mahmoud MHH, Mostafa NY. Recycling silica-rich wastes in sustainable mechanochemical-hydrothermal production of zeolite Y for ammonia remediation in aquaculture. J Sol-Gel Sci Technol (2023);106(1): 10-22. https://doi:10.1007/s10971-023-06066-1.
[45] Gado EAM, El-Deeb B, Ali EF, Mostafa NY, Bazaid SA. Evaluation of silver nanoparticles for the control of Phragmidium species in vitro and taif'rose rust disease in field. Res J Pharmaceut Bio Chem Sci (2016);7(3): 886-96.
[46] Nnanna L, Owate I. Electrochemical study of corrosion inhibition of mild steel in acidic solution using gnetum africana leaves extracts. Br J Appl Sci Technol (2015); 5(6): 556-67. https://doi:10.9734/bjast/2015/13605.
[47] Rajalakshmi KSV, Paari KA. A comprehensive study on the assessment of chemically modified Azolla pinnata as a potential cadmium sequestering agent. Int J Exp Res Rev (2023);36 1-19. https://doi:10.52756/ijerr.2023.v36.001.

[48] Singh A, Singh VK, Quraishi MA. Aqueous extract of kalmegh (andrographis paniculata) leaves as green inhibitor for mild steel in hydrochloric acid solution. Int J Corros (2010);2010: 1-10. https://doi:10.1155/2010/275983.
[49] Alvarez PE, Fiori-Bimbi MV, Neske A, Brandán SA, Gervasi CA. Rollinia occidentalis extract as green corrosion inhibitor for carbon steel in HCl solution. J Ind Eng Chem (2018);58: 92-9. https://doi:10.1016/j.jiec.2017.09.012.
[50] Riggs OL, Hurd RM. Temperature coefficient of corrosion inhibition. Corros (1967);23(8): 252-60. https://doi:10.5006/0010-9312-23.8.252.
[51] Kamel M, Hegazy M, Rashwan S, El Kotb M. Innovative surfactant of Gemini-type for dissolution mitigation of steel in pickling HCl media, Chin J Chem Eng (2021); 34: 125-33.
[52] Hegazy MA, Rashwan SM, Meleek S, Kamel MM. Synthesis, characterization, and mitigation action of innovative Schiff base on steel disintegration in sulfuric acid solution. Mater Chem Phys (2021); 267: 124697.
[53] Abdelfattah I, Abdelwahab W, El-Shamy A. Montmorillonitic clay as a cost effective, ecofriendly, and sustainable adsorbent for physicochemical treatment of contaminated water, Egypt J Chem (2022); 65(2): 687-94.
[54] Akinbulumo OA, Odejobi OJ, Odekanle EL. Thermodynamics and adsorption study of the corrosion inhibition of mild steel by Euphorbia heterophylla L. extract in 1.5 M HCl. Res Mater (2020);5 100074. https://doi:10.1016/j.rinma.2020.100074.
[55] Kamel MM, Rashwan SM, Mahmoud MAA, El-Mekawy SAA, Awad MK, Ibrahim HE. Resorcinol derivative as an environmentally friendly low carbon steel inhibitor in HCl medium. ACS Omega (2022);7(21): 17609-19. https://doi:10.1021/acsomega.2c00153.
[56] Chen L, Lu D, Zhang Y. Organic compounds as corrosion inhibitors for carbon steel in HCl solution: a comprehensive review. Materials (2022); 15: 2023. https://doi.org/10.3390/ma15062023.
[57] Mostafa NY, Montaser A, Al-Affray RA, Kamel MM, Alhadhrami A. Processing and characterization of novel calcium titanate/Na-titanate nanotube/rutile nanocomposite coating on titanium metal. Appl Phys A: Mater Sci Process (2019);125(5). https://doi:10.1007/s00339-019-2595-8.
[58] Bosch RW, Hubrecht J, Bogaerts WF, Syrett BC. Electrochemical frequency modulation: a new electrochemical technique for online corrosion monitoring. Corros (2001);57(1): 60-70. https://doi:10.5006/1.3290331.
[59] Obot IB, Onyeachu IB. Electrochemical frequency modulation (EFM) technique: theory and recent practical applications in corrosion research. J Mol Liq (2018);249: 83-96. https://doi:10.1016/j.molliq.2017.11.006.
[60] Kamel MM, Mohsen Q, Anwar ZM, Sherif MA. An expired ceftazidime antibiotic as an inhibitor for disintegration of copper metal in pickling HCl media. J Mater Res Technol (2021);11: 875-86. https://doi:10.1016/j.jmrt.2021.01.055.
[61] He Y, Wang X, Young D, Mohamed-Said M, Ren S, Singer M. Electrochemical study of corrosion inhibition of carbon steel during oil/water intermittent wetting. J Electrocheml Soc (2023);170(11): 111502. https://doi:10.1149/1945-7111/ad09f6.
[62] Raiedhah A. Alsaiari, Medhat M. Kamel, Mervate M. Mohamed, Corrosion Inhibition of Expired Cefazolin Drug on Copper Metal in Dilute Hydrochloric Acid Solution: Practical and Theoretical Approaches. Molecules 2024, 29, 1157. https://doi.org/10.3390/molecules29051157.
[63] Mu GN, Zhao TP, Liu M, Gu T. Effect of metallic cations on corrosion inhibition of an anionic surfactant for mild steel. Corros (1996);52(11): 853-56. https://doi:10.5006/1.3292077.
[64] Kamel M, Fouda AA, Rashwan S, Marei O. Burghul plant extract as a green corrosion inhibitor for carbon steel in hydrochloric acid solution. Catrina: Int J Environ Sci (2022);26(1): 19-31. https://doi:10.21608/cat.2022.277040.
[65] Emori W, Zhang R-H, Okafor PC, Zheng X-W, He T, Wei K, Lin X-Z, Cheng C-R. Adsorption and corrosion inhibition performance of multi-phytoconstituents from Dioscorea septemloba on carbon steel in acidic media: characterization, experimental and theoretical studies. Colloids Surf A: Physicochem Eng Asp (2020);590: 124534. https://doi:10.1016/j.colsurfa.2020.124534.
[66] Ahanotu CC, Onyeachu IB, Solomon MM, Chikwe IS, Chikwe OB, Eziukwu CA. Pterocarpus santalinoides leaves extract as a sustainable and potent inhibitor for low carbon steel in a simulated pickling medium. Sustain Chem Pharm (2020);15: 100196. https://doi:10.1016/j.scp.2019.100196.
[67] Abboud Y, Tanane O, Bouari AE, Salghi R, Hammouti B, Chetouani A, Jodeh S. Corrosion inhibition of carbon steel in hydrochloric acid solution using pomegranate leave extracts. Corros Eng Sci Technol (2016); 1-9. https://doi:10.1179/1743278215y.0000000058.
[68] Benabbouha T, Siniti M, El Attari H, Chefira K, Chibi F, Nmila R, Rchid H. Red algae halopitys incurvus extract as a green corrosion inhibitor of carbon steel in hydrochloric acid. J Bio Tribo Corros (2018);4(3). https://doi:10.1007/s40735-018-0161-0.
[69] Sobhy MA, Mahross MH, Abbas MA, ElZomrawyd A. Evaluation of Aloe vera gel extract as eco-friendly corrosion inhibitor for carbon steel in 1.0 M HCl, Egypt J Chem (2021); 64 (11): 6881- 89.

[70] Gado H, Albalawi MA. Experimental and theoretical investigations on the use of Corchorus olitorius stem extract as a safe corrosion inhibitor for carbon steel in hydrochloric acid. Egypt J Chem (2024) under press.
[71] Sidine MO , Lahbib H, Ba M , Salihi AMV, Benmessaoud M , Amor YB, Elemine BO. Corrosion inhibition of XC48 steel by Grewia bicolor jus leaves extract in 1M HCl acid medium: electrochemical and gravimetric study. Egypt J Chem (2024); 67 (4): 181-91.